

NLO QCD calculations with HELAC-NLO

G. Bevilacqua^a, M. Czakon^b, M. V. Garzelli^{cd}, A. van Hameren^e, Y. Malamos^f, C. G. Papadopoulos^a, R. Pittau^c and M. Worek^g

^aInstitute of Nuclear Physics, NCSR "Demokritos", GR-15310 Athens, Greece

^bInstitut für Theoretische Physik E, RWTH Aachen University D-52056 Aachen, Germany

^cDepartamento de Física Teórica y del Cosmos y CAFPE, E-18071 Granada, Spain

^dINFN Milano, I-20133 Milano, Italy

^eInstitute of Nuclear Physics, Polish Academy of Sciences, PL-31342 Cracow, Poland

^fDepartment of Theoretical High Energy Physics, Institute for Mathematics, Astrophysics and Particle Physics, Radboud Universiteit Nijmegen, 6525 AJ Nijmegen, the Netherlands

^gFachbereich C Physik, Bergische Universität Wuppertal, D-42097 Wuppertal, Germany

Achieving a precise description of multi-parton final states is crucial for many analyses at LHC. In this contribution we review the main features of the HELAC-NLO system for NLO QCD calculations. As a case study, NLO QCD corrections for $t\bar{t} + 2$ jet production at LHC are illustrated and discussed.

1. Introduction

With the successful start of collisions at 7 TeV a few months ago, the Large Hadron Collider has put another milestone towards a thorough exploration of the Terascale. The large energy available will open many multi-particle channels that have been widely investigated [1]. In view of a correct interpretation of the signals of new physics which might be extracted from data, it is of considerable interest to reduce our theoretical uncertainty for the physical processes under study, especially when large QCD backgrounds are involved. In this respect, the need of Next-to-Leading-Order (NLO) corrections for the LHC is unquestionable.

Many efforts have been made in the last few years in developing efficient techniques for one-loop calculations, using both highly-refined traditional methods and the new approaches of OPP and Generalized Unitarity. A significant achievement of this work has been the calculation of complete NLO predictions for several interesting

$2 \rightarrow 4$ processes at LHC [2,3,4,5,6,7,8,9,10].

In this contribution we describe the main features of the HELAC-NLO approach to NLO calculations. We provide an overview of the computational framework and briefly summarize some physics results obtained with this system.

2. Structure of HELAC-NLO

2.1. Virtual corrections

The calculation of the virtual corrections is organized in the framework of the OPP method.

Any one-loop amplitude is characterized by a set of denominators given as products of loop propagators, $\bar{D}_i(\bar{q}) = (\bar{q} + p_i)^2 - m_i^2$, and a polynomial – in the loop momentum – function called numerator, $\bar{N}_I(\bar{q})$, such that it can be represented in the form

$$\mathcal{A} = \sum_{I \subset \{1, \dots, n\}} \int \frac{\mu^{4-d} d^d \bar{q}}{(2\pi)^d} \frac{\bar{N}_I(\bar{q})}{\prod_{i \in I} \bar{D}_i(\bar{q})}, \quad (1)$$

where both the loop momentum \bar{q} and the numerator function are considered to be evaluated in d

dimensions. On the other hand, it is well known that any one-loop amplitude admits a decomposition in terms of a basis of d -dimensional scalar integrals. In the limit $d \rightarrow 4$, this decomposition can be cast into the form

$$\begin{aligned} \mathcal{A} &= \sum_i d_i \text{Box}_i + \sum_i c_i \text{Triangle}_i \\ &+ \sum_i b_i \text{Bubble}_i + \sum_i a_i \text{Tadpole}_i + R, \quad (2) \end{aligned}$$

where Box, Triangle, Bubble and Tadpole denote the known scalar loop functions and R is a rational function in the invariants also known as rational term.

The basic idea of OPP is to decompose the numerator of the integrand function, $N(q)$, into a basis of monomials of the propagators appearing in the denominator: the coefficients of the expansion are the a, b, c, d appearing in Eq.2 plus additional, q -dependent, coefficients also known as spurious terms, whose analytical dependence on the loop momentum is known. It is therefore possible to evaluate the coefficients of the expansion by computing $N(q)$ a sufficient number of times (equal the number of coefficients to be determined), by appropriate choices of q . One possibility is to select those values of the loop momentum that nullify certain sets of propagators – the so-called unitarity cuts – and solve the resulting linear system of equations in terms of the expansion coefficients. If the numerator $N(q)$ is considered in $d = 4$ dimensions, it is necessary to decompose the rational terms, $R = R_1 + R_2$: we call R_1 the part of the rational terms that is derived through the reduction starting with a $d = 4$ numerator function. R_2 is the part of the rational terms that originates from the explicit $(d - 4)$ dependence of the numerator function evaluated in d dimensions. As has been proven in [12] R_2 can be fully determined by including new interaction-vertices with up to four legs, in full similarity with the usual UV counter-terms.

On the one hand the method can be fully implemented numerically, resulting to a very fast reduction of arbitrary multi-leg amplitudes. On the other hand, being inherently algebraic, provides exact results (with arbitrary precision) for the coefficients multiplying the one-loop scalar func-

tions as well as for the rational terms. The OPP method thus provides a systematic framework to evaluate the cut-constructible part of the amplitude as well as the R_1 term, given a numerator function as input (see [11,12] for details).

In the approach we follow **HELAC-1LOOP** [14], based on **HELAC-PHEGAS** [13], automatically generates all the input numerators for the OPP reduction as well as all tree-order-like contributions including the new vertices needed for the full determination of the rational part (R_2) [15,16], as well as UV-renormalization counter-terms. For a detailed description of the algorithm we refer to [14].

To summarize, our approach for the evaluation of one-loop amplitudes relies upon three basic elements: 1) an implementation of the OPP reduction; 2) a library of scalar loop integrals; 3) an algorithm to automatically evaluate numerator functions and R_2 terms. These tasks are solved respectively by the codes **CutTools**, **OneL0op** and **HELAC-1LOOP** [22,14].

We organize the calculation of virtual corrections using a re-weighting technique and adopt helicity and colour sampling methods in order to optimize the performance of our system [5].

The treatment of the QCD colour is based on the colour connection representation. Given a generic QCD amplitude, $\mathcal{M}_{j_1 \dots j_{n_q}}^{i_1 \dots i_{n_q}, a_1, \dots, a_{n_g}}$, composed by n_g gluons and n_q quarks (antiquarks) with colour indices a and i (j) respectively, it is possible to get a uniform representation for quarks and gluons by contracting each gluon index a with a corresponding t_{ij}^a :

$$\mathcal{M}_{j_1 \dots j_{n_q}}^{i_1 \dots i_{n_q}, a_1, \dots, a_{n_g}} \rightarrow \mathcal{M}_{j_1 \dots j_{n_q+n_g}}^{i_1 \dots i_{n_q+n_g}} \quad (3)$$

The resulting amplitude can be now decomposed in terms of colour-stripped partial amplitudes A_σ :

$$\mathcal{M}_{j_1, j_2, \dots, j_k}^{i_1, i_2, \dots, i_k} = \sum_{\sigma} \delta_{i_{\sigma_1}, j_1} \delta_{i_{\sigma_2}, j_2} \dots \delta_{i_{\sigma_k}, j_k} A_{\sigma}, \quad (4)$$

with $k = n_q + n_g$, and σ denoting a permutation of the set $\{1, \dots, k\}$. Each A_σ is interpreted as the contribution to the amplitude associated to one possible way of connecting the external particles through colour flow, the connection being established by the indices of the δ 's. The Feyn-

man rules that allow the calculation of all A_σ 's have been described in Refs. [23,24,13].

At the level of squared matrix element, the following equivalence holds:

$$\sum_{\{i\},\{j\}} |\mathcal{M}_{j_1,j_2,\dots,j_k}^{i_1,i_2,\dots,i_k}|^2 = \sum_{\sigma,\sigma'} A_\sigma^* \mathcal{C}_{\sigma,\sigma'} A_{\sigma'} , \quad (5)$$

where the colour matrix, $\mathcal{C}_{\sigma,\sigma'}$, can be evaluated automatically by counting the number of cycles that are obtained by closing the colour flows of σ, σ' . Full colour summation is performed using the right-hand side of Eq. 5.

While appealing, the colour-connection representation has a drawback in that the computation becomes less efficient for processes with high parton multiplicities. Indeed, the number of partial amplitudes that have to be evaluated for a given phase-space point increases factorially with the number of the external coloured particles. A possible way out is given by the colour sampling approach where, following the left hand side of Eq. 5, one generates for each phase-space point a random colour assignment and computes the matrix element $\mathcal{M}_{j_1,j_2,\dots,j_k}^{i_1,i_2,\dots,i_k}$ accordingly: due to Eq.4, only the subset of the A_σ 's which have a colour flow compatible with the given assignment contribute. In fact, as shown in Table 1, the number of subamplitudes that have to be computed in this way is sensibly reduced, on the average, for increasing complexity of the colour structure.

2.2. Real corrections

The singularities arising from soft and collinear divergences in the initial and final states are treated within the framework of Catani-Seymour dipole subtraction [25], in its formulation for massive quarks [26] and arbitrary polarizations [27]. After combining virtual and real corrections, singularities connected to collinear configurations in the final state as well as soft divergencies in the initial and final state automatically cancel for infrared-safe observables when the jet algorithm is applied. Singularities connected to collinear splittings in the initial state are removed via PDF factorization.

Calculations are performed with the help of the code `HELAC-DIPOLES` [27] which implements automatic construction of all relevant subprocesses

and dipoles as well as phase-space integration of subtracted real radiation and of the corresponding integrated dipoles. The phase-space integration is performed using the approaches of the multichannel generator `PHEGAS` [28] and of the recently published adaptive-multichannel generator `KALEU` [29].

A phase-space restriction is applied on the contribution of dipoles, as originally proposed in [30,31], considering two values of the unphysical cutoff: $\alpha_{max} = 1$ and $\alpha_{max} = 0.01$. The α_{max} independence is explicitly checked in all our results as a consistency check of the calculation.

3. Predictions for the LHC: $t\bar{t} + 2$ jets

The `HELAC-NLO` framework has been applied in the computation of NLO QCD corrections to several processes relevant for top quark and Higgs phenomenology [1,5,9]. We report here, as an example, a brief summary of our results about inclusive production of $t\bar{t}$ in association with two jets, which represents an important background for Higgs searches in the channel $t\bar{t}H(H \rightarrow b\bar{b})$ [32].

To be specific, we consider proton-proton collisions at the center of mass energy $\sqrt{s} = 14$ TeV. Top quarks are considered on shell without any kinematical restriction applied. For the top quark mass we set $m_t = 172.6$ GeV, whereas all the other partons are considered massless. We consistently use the CTEQ6 set of parton distribution functions throughout the calculation, *i.e.* we take the CTEQ6L1 set with a one-loop running α_S at LO and CTEQ6M pdf's with a two-loop running α_S for the evaluation of the NLO corrections.

Our definition of jets is based on the k_T algorithm [33,34] using $\Delta R = 0.8$, where ΔR denotes the separation in the azimuthal angle - pseudorapidity plane. Jets are obtained by recombining at most two partons and the recombination takes place only when both partons satisfy $|y_i| < 5$ (approximate detector bounds). Also b quarks enter our jet definition, so the final state $t\bar{t}b\bar{b}$ is included in the analysis. We further impose a minimum $\Delta R = 1.0$ separation between jets and require the latter to lie within the region defined by $|y_{jet}| < 4.5$. Finally, we require hard jets to have a minimum transverse momentum of 50 GeV.

Table 1

Comparison between the number of subamplitudes to be evaluated using full colour sum (n_{conn}) and using the Monte Carlo approach described in the text (average number, $\langle n_{conn} \rangle_{MC}$), for three reference processes.

Process	n_{conn}	$\langle n_{conn} \rangle_{MC}$	Ratio
$gg \rightarrow b\bar{b}W^+W^-$	6	1.74	3.5
$gg \rightarrow t\bar{t}b\bar{b}$	24	3.04	7.89
$gg \rightarrow t\bar{t}gg$	120	6.27	19.1

The numerical results of this study are summarized in Table 2, where we show a comparison of the total LO and NLO cross sections at the central scale $\mu_R = \mu_F = m_t$. As a cross check, we report the NLO results obtained for two different values of the dipoles cutoff parameter, $\alpha_{max} = 1$ and $\alpha_{max} = 0.01$, showing that they are in mutual agreement within the integration error.

The scale dependence of the corrections is illustrated in Figure 1. In the absence of any jet veto, QCD corrections determine a negative shift of approximately 11% compared to the LO results. A dramatic reduction of the scale uncertainty is observed when going from LO to NLO: varying the scale up and down by a factor 2 changes the LO cross section by +72% and -39% respectively, while in the NLO case one observes a variation of -13% and -12%. Applying a jet veto of 50 GeV results in an increasing negative shift operated by QCD corrections and leads to a K-factor of 0.64.

Let us now analyse the changes in shape of distributions determined by QCD corrections. A few differential cross sections for simple observables are considered. The most important one for us is the di-jet invariant mass since it is the observable entering Higgs boson studies. This is illustrated in Figure 2, where we focus the attention in the range up to 400 GeV due to our phenomenological motivations. We notice that the distribution shows tiny corrections up to at least 200 GeV.

Much larger effects can be found in the other observables analysed, namely the transverse momentum of the first and of the second hardest jet. Figures 3 and 4 show visible differences in shape in the region of high p_T , especially in the case of the first hardest jet. We conclude by pointing out that an accurate description of the tails of these

p_T distributions cannot prescind from the inclusion of higher-order corrections. On the other hand, the behaviour at low p_T 's is altered by soft collinear emissions whose effects can be simulated by parton showers.

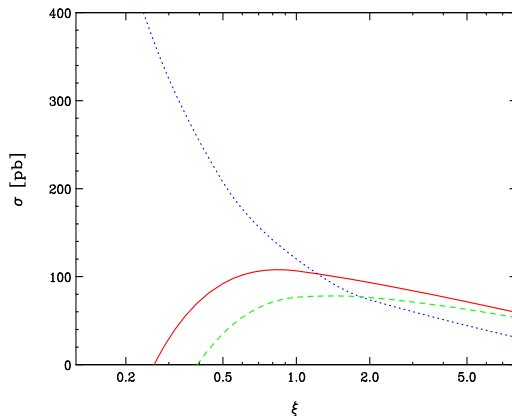


Figure 1. Scale dependence of the total cross section for $pp \rightarrow t\bar{t} + 2 \text{ jets} + X$ at the LHC with $\mu_R = \mu_F = \xi \mu_0$, where $\mu_0 = m_t$. The blue dotted curve corresponds to the LO, the red solid to the NLO result whereas the green dashed to the NLO results with a jet veto of 50 GeV.

4. Outlook

It is amazing how much progress has been realized over the last few years in the field of multi-leg NLO calculations. HELAC-NLO is a complete

Table 2

Cross section at LO and NLO for $t\bar{t} + 2$ jets production at LHC ($\sqrt{s} = 14$ TeV). The two NLO results reported refer to different values of the dipole phase-space cutoff α_{max} . The scale choice is $\mu_R = \mu_F = m_t$.

$pp \rightarrow t\bar{t} + 2$ jets + X	σ^{LO} (pb)	$\sigma_{\alpha_{max}=1}^{\text{NLO}}$ (pb)	$\sigma_{\alpha_{max}=0.01}^{\text{NLO}}$ (pb)
no jet veto	120.17 ± 0.08	106.95 ± 0.17	106.56 ± 0.31
with jet veto ($p_{T,X} < 50$ GeV)	120.17 ± 0.08	76.58 ± 0.17	76.57 ± 0.37

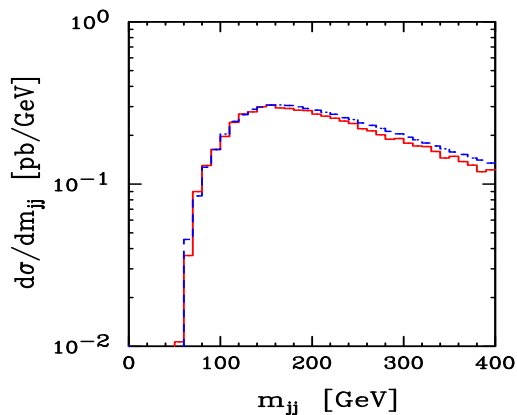


Figure 2. Distribution of the di-jet invariant mass for $pp \rightarrow t\bar{t} + 2$ jets + X at the LHC. The red solid line refers to the NLO results while the blue dotted one to the LO one.

framework for NLO calculations, including virtual and real corrections. In its present form can be used for NLO QCD calculations for arbitrary processes including up to one-particle-irreducible 8-point one-loop functions. It has been successfully used for a number of processes of current interest, such as $pp \rightarrow t\bar{t}b\bar{b}$ including the Higgs signal contributions and $pp \rightarrow t\bar{t} + 2$ jets. In the immediate future, we plan a complete analysis of $t\bar{t}$ -jets production including the full description of top decays and non-resonant contributions, i.e. $pp \rightarrow l\bar{\nu}l'\nu'bb$. Plans of further development include also the incorporation of all R_2 and UV counter-terms for full electroweak corrections.

Acknowledgement: This work was funded in part by the RTN European Programme MRTN-CT-2006-035505 HEP-TOOLS - Tools and Precision Calculations for Physics Dis-

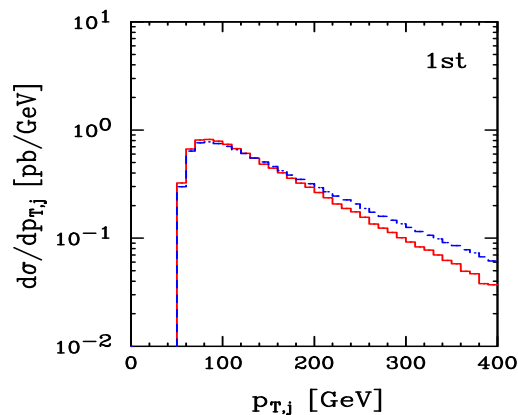


Figure 3. Distributions of the transverse momentum for the first hardest jet for $pp \rightarrow t\bar{t} + 2$ jets + X at the LHC. The red solid line refers to the NLO results while the blue dotted one to the LO one.

coveries at Colliders. M.C. was supported by the Heisenberg Programme of the Deutsche Forschungsgemeinschaft. M.W. was supported by the Initiative and Networking Fund of the Helmholtz Association, contract HA-101 ("Physics at the Terascale"). M.V.G. and R.P. thank the financial support of the MEC project FPA2008-02984. M.V.G. was additionally supported by the INFN.

REFERENCES

1. J. R. Andersen *et al.* [SM and NLO Multileg Working Group], arXiv:1003.1241 [Unknown].
2. R. Keith Ellis, K. Melnikov and G. Zanderighi, Phys. Rev. D **80** (2009) 094002 [arXiv:0906.1445 [hep-ph]].
3. C. F. Berger *et al.*, Phys. Rev. D **80** (2009)

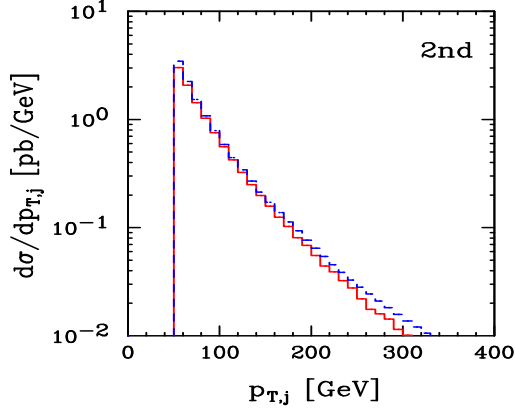


Figure 4. Distributions of the transverse momentum for the second hardest jet for $pp \rightarrow t\bar{t} + 2 \text{ jets} + X$ at the LHC. The red solid line refers to the NLO results while the blue dotted one to the LO one.

- 074036 [arXiv:0907.1984 [hep-ph]].
4. A. Bredenstein, A. Denner, S. Dittmaier and S. Pozzorini, Phys. Rev. Lett. **103** (2009) 012002 [arXiv:0905.0110 [hep-ph]].
5. G. Bevilacqua, M. Czakon, C. G. Papadopoulos, R. Pittau and M. Worek, JHEP **0909** (2009) 109 [arXiv:0907.4723 [hep-ph]].
6. K. Melnikov and G. Zanderighi, Phys. Rev. D **81** (2010) 074025 [arXiv:0910.3671].
7. T. Binoth, N. Greiner, A. Guffanti, J. Reuter, J. P. Guillet and T. Reiter, Phys. Lett. B **685** (2010) 293 [arXiv:0910.4379].
8. A. Bredenstein, A. Denner, S. Dittmaier and S. Pozzorini, JHEP **1003** (2010) 021 [arXiv:1001.4006 [Unknown]].
9. G. Bevilacqua, M. Czakon, C. G. Papadopoulos and M. Worek, Phys. Rev. Lett. **104** (2010) 162002 [arXiv:1002.4009].
10. C. F. Berger *et al.*, arXiv:1004.1659.
11. G. Ossola, C. G. Papadopoulos and R. Pittau, Nucl. Phys. B **763** (2007) 147 [arXiv:hep-ph/0609007].
12. G. Ossola, C. G. Papadopoulos and R. Pittau, JHEP **0805** (2008) 004 [arXiv:0802.1876 [hep-ph]].
13. A. Cafarella, C. G. Papadopoulos and M. Worek, Comput. Phys. Commun. **180** (2009) 1941 [arXiv:0710.2427 [hep-ph]].
14. A. van Hameren, C. G. Papadopoulos and R. Pittau, JHEP **0909** (2009) 106 [arXiv:0903.4665 [hep-ph]].
15. P. Draggiotis, M. V. Garzelli, C. G. Papadopoulos and R. Pittau, JHEP **0904** (2009) 072 [arXiv:0903.0356 [hep-ph]].
16. M. V. Garzelli, I. Malamos and R. Pittau, JHEP **1001** (2010) 040 [arXiv:0910.3130].
17. W. T. Giele, Z. Kunszt and K. Melnikov, JHEP **0804** (2008) 049 [arXiv:0801.2237 [hep-ph]].
18. R. K. Ellis, W. T. Giele, Z. Kunszt and K. Melnikov, Nucl. Phys. B **822** (2009) 270 [arXiv:0806.3467 [hep-ph]].
19. A. Lazopoulos, arXiv:0812.2998 [hep-ph].
20. R. Britto, F. Cachazo and B. Feng, Nucl. Phys. B **725** (2005) 275 [arXiv:hep-th/0412103].
21. C. Anastasiou, R. Britto, B. Feng, Z. Kunszt and P. Mastrolia, Phys. Lett. B **645** (2007) 213 [arXiv:hep-ph/0609191].
22. G. Ossola, C. G. Papadopoulos and R. Pittau, JHEP **0803** (2008) 042 [arXiv:0711.3596 [hep-ph]].
23. A. Kanaki and C. G. Papadopoulos, Comput. Phys. Commun. **132** (2000) 306 [arXiv:hep-ph/0002082].
24. A. Kanaki and C. G. Papadopoulos, arXiv:hep-ph/0012004.
25. S. Catani and M. H. Seymour, Nucl. Phys. B **485** (1997) 291 [Erratum-ibid. B **510** (1998) 503] [arXiv:hep-ph/9605323].
26. S. Catani, S. Dittmaier, M. H. Seymour and Z. Trocsanyi, Nucl. Phys. B **627** (2002) 189 [arXiv:hep-ph/0201036].
27. M. Czakon, C. G. Papadopoulos and M. Worek, JHEP **0908** (2009) 085 [arXiv:0905.0883 [hep-ph]].
28. C. G. Papadopoulos, Comput. Phys. Commun. **137** (2001) 247 [arXiv:hep-ph/0007335].
29. A. van Hameren, arXiv:1003.4953 [Unknown].
30. Z. Nagy and Z. Trocsanyi, Phys. Rev. D **59** (1999) 014020 [Erratum-ibid. D **62** (2000) 099902] [arXiv:hep-ph/9806317].
31. Z. Nagy, Phys. Rev. D **68** (2003) 094002

- [arXiv:hep-ph/0307268].
32. The ATLAS Collaboration (G. Aad *et al.*), arXiv:0901.0512v4 [hep-ex]
 33. S. Catani, Y. L. Dokshitzer and B. R. Webber, Phys. Lett. B **285**, 291 (1992).
 34. S. Catani, Y. L. Dokshitzer, M. H. Seymour and B. R. Webber, Nucl. Phys. B **406**, 187 (1993).